Ab initio quantum force field for simulations of nanostructures

A. G. Donchev*
Algodign, LLC, Bolshaya Sadovaya 8, Moscow 123001, Russia
(Received 3 October 2006; published 1 December 2006; corrected 4 December 2006)

It is demonstrated that the third generation of a recently introduced quantum mechanical polarizable force field (QMPFF) successfully reproduces experimental data on binding energies of polycyclic aromatic hydrocarbons and fullerene C_{60} with graphite. The QMPFF also provides an accurate description of bulk graphite and solid C_{60} properties. In all the studied systems, the electrostatics due to the penetration effect was found to be important and comparable in magnitude with the total interaction energy. The QMPFF predicts graphite exfoliation energy of 55 meV/atom in agreement with the relatively large experimental value of 52±5 meV/atom recently suggested by Zacharia *et al.* [Phys. Rev. B **69**, 155406 (2004)].

DOI: 10.1103/PhysRevB.74.235401 PACS number(s): 81.05.Uw, 61.48.+c, 61.50.Lt, 68.43.−h

I. INTRODUCTION

Since the pioneering work of Girifalco and Lad[1] empirical force fields (FFs) have been widely used in simulations of interacting carbon structures, such as fullerenes, nanotubes, and their common progenitor, the graphene layer. To possess predictive power, the empirical FFs should be parametrized against a reliable set of experimental data. The most important of these is the graphite exfoliation energy E_{ex} needed to separate a single graphene layer from its parent crystal,[39] because this quantity is a direct measure of the weak van der Waals forces between carbons.

Unfortunately, despite all the technical progress of the last 50 years, the precise value of E_{ex} remains poorly defined. Due to the layered nature of graphite, its total heat of sublimation characterizes primarily the intralayer C-C chemical bonds, two orders of magnitude stronger than the desired E_{ex}. As the conventional techniques fail, experimentalists have tried to contrive alternatives, but no consensus has yet been achieved. The experimental range for E_{ex} extends from 25 to nearly 60 meV/atom.[2,3] At the same time the theoretical predictions are also rather uncertain. The density functional theory (DFT) values for E_{ex} are even more variable than the experimental: from almost zero to more than 100 meV/atom.[4] A more rigorous *ab initio* quantum method, coupled cluster singles, doubles, and perturbative triples [CCSD(T)] for example, could clarify this issue. But at the present time the CCSD(T) method is too computationally intensive to be directly applied to graphite.

An attractive alternative is a FF parametrized against high-level *ab initio* quantum mechanical (QM) data for systems that are relatively small but possess all the distinctive features of graphene. This approach has proved to be very successful in bio- and chemical physics. An additional advantage of such a quantum FF is the opportunity to study the interaction of carbon structures with noncarbon objects, e.g., molecular hydrogen, water, and ions. All these examples are very interesting from both the theoretical and applied-science points of view;[5–8] it is enough to mention only the problem of hydrogen storage and transportation.[9–11]

The most graphenelike class of compounds that can form a training set for a quantum FF are the polycyclic aromatic hydrocarbons (PAHs).[12] A PAH can be considered as a fragment of a graphene layer [see Fig. 1(a)] with the peripheral atoms covalently bonded to hydrogens. The main concern in designing the quantum FF should be transferability, especially in the case of carbon nanostructures, because of a limited set of reliable data for validation of the model. Relatively early the special significance of the electrostatic (ES) interaction for PAHs was realized. It is the ES component that is responsible both for the relative stability of the T-shaped conformation of the benzene dimer and for the herringbone crystal structure peculiar to all PAHs.[13] Hence, the usual choice for nano-FFs of the simplest Lennard-Jones functional form (or something similar) is inappropriate. However, even the correct reproduction of the quadrupole moments of PAHs (as a rule, their dipoles are zero by symmetry) does not guarantee the desired transferability. For example, the point-charge model fails to explain even qualita-

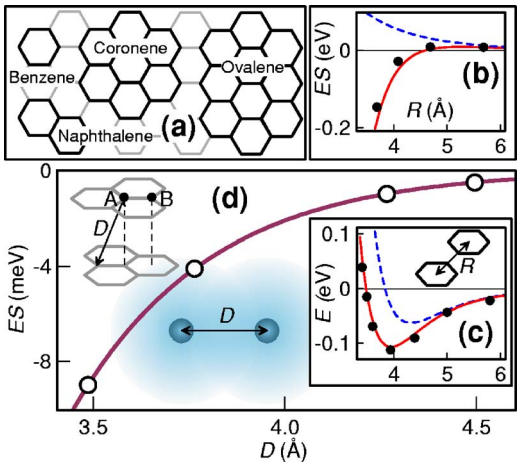

FIG. 1. (Color online) (a) PAHs are presented as fragments of a graphene layer. (b) Electrostatic energy component for PD benzene dimer. QMPFF results (solid red line) are compared with point-charge MMFF94 (Ref. 14) (dashed blue line) and QM data (filled black circles) calculated at second-order Møller-Plesset perturbation theory (MP2) level. (c) Same as (b), but for the total interaction energy. The QM values are the CCSD(T) results (Refs. 18 and 19). (d) ES energy calculated with the QMPFF (which is nonzero due to the interpenetration of electron clouds) for a pair of neutral graphite carbons. Open circles correspond to the actual, discrete separations of atoms in adjacent layers.

TABLE I. QMPFF atom-type parameters (in atomic units) for PAHs. The same carbon parameters are used for both graphite and fullerene.

A	α_A	Z_A	w_A	$\ln C_A^{EX}$	u_A	$\ln C_A^{DS6}$	$\ln C_A^{DS8}$
C	8.04	2	0.5750	1.90	0.5848	1.60	3.20
H	2.28	1	0.3834	0.90	0.4923	0.57	1.73

TABLE II. QMPFF bond-type parameters (in atomic units) for PAHs. The same CC bond parameters are used for both graphite and fullerene.

AB	s_{AB}	s_{BA}	t_{AB}	t_{BA}	Q_{AB}	Q_{BA}	R_{AB}
CC	−0.0586	−0.0586	0.04	0.04	−0.0173	−0.0173	2.64
CH	0.0000	0.0000	0.06	0.04	−0.0276	0.0000	2.04

tively the distance dependence of the ES energy for the parallel-displaced (PD) conformation of the benzene dimer [see Fig. 1(b)]. Elucidation of this dependence strongly requires accounting for the so-called penetration effect arising from overlap of the electron clouds.

In this paper it is demonstrated that QMPFF,[15–17] fitted to the state-of-the-art CCSD(T) results for the benzene dimer, successfully reproduces basic experimental findings on properties of bulk graphite and solid C_{60}, as well as the PAH-graphite binding energies measured recently.[3] This two-sided agreement of the QMPFF results both with QM and with experiment, has broad scientific significance as it validates the CCSD(T)-experiment consistency, which is extremely difficult to test directly. Also, the QMPFF prediction for the graphite E_{ex} (which we believe will turn out to be close to the true QM value, when the latter can be calculated) will be very useful for resolution of the semicentennial controversy mentioned above.

II. METHODS

A. Charge density

The QMPFF method starts from the careful modeling of the charge density, which is written for atom a belonging to type A and located at position $\mathbf{R}_a$ as

$$\rho_a(\mathbf{r}) = Z_A \delta(\mathbf{r} - \mathbf{R}_a) + \mathcal{D}_a \frac{q_a}{8\pi w_A^3} \exp(-|\mathbf{r} - \mathbf{R}_a|/w_A). \quad (1)$$

In this equation the three-dimensional Dirac δ function corresponds to the point positive atomic core representing the nucleus and compact inner electron shells. The core charge Z_A is the model parameter and depends only on the type A. This rule is valid for all the parameters with capitalized index, in contrast with lower-case subscripts, which denote the dependence on a particular atom. The second summand in Eq. (1) stands for the diffuse cloud of negative charge, which represents in a simplified but reasonable fashion the outer electrons. Thus the penetration electrostatic effect can be naturally accounted for. Both the cloud's size w_A and its integral charge q_a are model parameters. For all the systems considered in current research total neutrality is provided by the relation $q_a = -Z_A$, however this equality can be violated in polar molecules, e.g., water, because of chemical bond charge transfer.[15,16]

The differential operator $\mathcal{D}_a$ in Eq. (1) is defined as

$$\mathcal{D}_a = 1 + \mathbf{t}_a \frac{\partial}{\partial \mathbf{R}_a} + \frac{1}{2}\left(\frac{\partial}{\partial \mathbf{R}_a}\right)^T \boldsymbol{\omega}_a \frac{\partial}{\partial \mathbf{R}_a}, \quad (2)$$

where the vector $\mathbf{t}_a$ and 3×3 traceless tensor $\boldsymbol{\omega}_a$ introduce, respectively, the local dipole and quadrupole in the form of p- and d-type density anisotropy. The vector $\mathbf{t}_a$ is a sum of permanent and induced components

$$\mathbf{t}_a = \mathbf{t}_a^{per} + \mathbf{t}_a^{ind}. \quad (3)$$

The permanent part is written as a sum over the set $\{a\}$ of all the chemical neighbors of atom a:

$$\mathbf{t}_a^{per} = \sum_{b\in\{a\}} t_{AB} \mathbf{R}_{ab}, \quad (4)$$

where $\mathbf{R}_{ab} = \mathbf{R}_b - \mathbf{R}_a$ and t_{AB} is the QMPFF bond-type parameter (note that generally $t_{AB} \neq t_{BA}$). The induced part in Eq. (3) is written as

$$\mathbf{t}_a^{ind} = t^{max} \boldsymbol{\tau}_a, \quad (5)$$

where the parameter $t^{max} = 0.2$ a.u. and the dimensionless vector $\boldsymbol{\tau}_a$ represents the QMPFF dynamic variable. The length τ_a is confined within the interval $0 \leqslant \tau_a < 1$ by the restraint potential (see below).

As for the local quadrupole tensor, its components are calculated as

$$\omega_{a,\alpha\beta} = \sum_{b\in\{a\}} Q_{AB}(R_{ab,\alpha}R_{ab,\beta} - \delta_{\alpha\beta}R_{ab}^2/3), \quad (6)$$

where $\alpha, \beta = x, y, z$ and Q_{AB} is the bond-type parameter (generally $Q_{AB} \neq Q_{BA}$). The negative (positive) sign of Q_{AB} corresponds to oblate (prolate) deformation of the cloud's shape along the chemical bond. It is interesting to note that Q_{AB} was found to be negative or zero for all the parametrized bond types (not only those presented in this paper). For example, the expected out-of-plane elongation of the electron density around an aromatic carbon results from the contraction along the three chemical bonds it participates in.

B. Potentials

The total potential energy of the system is a sum (minimized over the dynamic variables) of pairwise electrostatics, exchange repulsion (EX), and dispersion (DS), and also the unary restraint term:

$$U = \min_{\tau} \left\{ \sum_{a,b}{}' (U_{ab}^{\mathrm{ES}} + U_{ab}^{\mathrm{EX}} + U_{ab}^{\mathrm{DS}}) + \sum_a U_a^{IN} \right\}. \quad (7)$$

The prime in the first sum indicates the usual omission of the self-terms $a=b$ and the atomic pairs separated by one or two chemical bonds.

TABLE III. QMPFF predictions for optimal graphene layer separation R_0, interaction energy E, and its components: electrostatics (ES), exchange (EX), and dispersion (DS). The intralayer lattice constant is fixed at the experimental value of 2.46 Å (Ref. 23), which corresponds to a C-C bond length of 1.42 Å. All energies are in meV/atom.

System	Stacking	R_0 (Å)	E	ES	EX	DS
Two layers	*AB*	3.519	−49.9	−42.5	66.9	−74.3
Two layers	*AA*	3.563	−47.9	−38.2	60.9	−70.6
Bulk	*AB*	3.486	−54.9	−46.1	73.6	−82.5
Bulk	*AA*	3.532	−52.7	−41.3	66.9	−78.2

The electrostatic component includes cloud-cloud, cloud-core, and core-core contributions

$$U_{ab}^{ES} = q_a q_b \mathcal{D}_a \mathcal{D}_b \varphi(R_{ab}; w_A, w_B) + Z_A q_b \mathcal{D}_b \varphi(R_{ab}; 0, w_B) + q_a Z_B \mathcal{D}_a \varphi(R_{ab}; w_A, 0) + Z_A Z_B / R_{ab}, \quad (8)$$

where $\mathcal{D}_a$ is the differential operator defined in (2) and the potential between two exponentially shaped spherical clouds is

$$\varphi(r;\mu,\nu) = \frac{1}{r}[1 - f(r;\mu,\nu)e^{-r/\mu} - f(r;\nu,\mu)e^{-r/\nu}],$$

$$f(r;\mu,\nu) = \frac{\mu^4(3\nu^2 - \mu^2)}{(\nu^2 - \mu^2)^3} + \frac{\mu^3}{2(\nu^2 - \mu^2)^2} r.$$

Two limiting cases are also useful:

$$\varphi(r;\mu,\mu) = \frac{1}{r}\left[1 - \frac{1}{48}e^{-r/\mu}\left(\frac{r^3}{\mu^3} + 9\frac{r^2}{\mu^2} + 33\frac{r}{\mu} + 48\right)\right],$$

$$\varphi(r;\mu,0) = \frac{1}{r}\left[1 - \frac{1}{2}e^{-r/\mu}\left(\frac{r}{\mu} + 2\right)\right].$$

The exchange repulsion acts only between clouds,

$$U_{ab}^{EX} = C_A^{EX} C_B^{EX} \mathcal{D}_a \mathcal{D}_b \chi(R_{ab}; u_A, u_B), \quad (9)$$

where C_A^{EX} and u_A are specific model parameters, and

$$\chi(r;\mu,\nu) = \frac{e^{-r/\nu} - e^{-r/\mu}}{r/\mu - r/\nu}.$$

In the limit of two identical sizes we have the familiar Born-Mayer exponent

$$\chi(r;\mu,\mu) = e^{-r/\mu}.$$

It is worth noting that the cloud-cloud character of the exchange repulsion allows our model to account for exchange nonadditivity, which is almost always neglected by other polarizable FFs.

The dispersion involves only cores and is therefore independent of the dynamic variables:

$$U_{ab}^{DS} = -C_A^{DS6} C_B^{DS6} \frac{\psi_6(R_{ab}/v)}{R_{ab}^6} - C_A^{DS8} C_B^{DS8} \frac{\psi_8(R_{ab}/v)}{R_{ab}^8}, \quad (10)$$

where C_A^{DS6} and C_A^{DS8} are the force constants, and the ψ's are the Tang-Toennies[20] damping functions with common size $v = 0.6$ a.u.:

$$\psi_n(x) = 1 - e^{-x}\sum_{k=1}^{n} \frac{x^k}{k!}.$$

The restraint potential has the form of an anharmonic spring:

$$U_a^{IN} = \frac{(q_a t_A^{max})^2}{\alpha_A} \frac{1 + \sum_{b\in\{a\}} s_{AB}(\boldsymbol{\tau}_a \mathbf{R}_{ab})^2}{1 + \sum_{b\in\{a\}} s_{AB} R_{AB}^2/3} (1 - \sqrt{1 - \tau_a^2}), \quad (11)$$

where α_A corresponds to the isotropic polarizability of the atom type, while s_{AB} is an anisotropic contribution along the chemical bond with the reference bond length R_{AB} (note that $R_{AB} = R_{BA}$, while generally $s_{AB} \neq s_{BA}$). For all the parametrized atomic types the values of s_{AB} were found to be nonpositive, which implies greater polarizability in the direction parallel to the bond than in the perpendicular one. In the case of sp^2 symmetry this straightforwardly results in the well-known damping of the out-of-plane polarizability component.

It is easy to see that the right-hand side of both Eq. (8) and Eq. (9) is a quadratic form in the variables $\mathbf{t}_a$ (and hence $\boldsymbol{\tau}_a$). However, the anharmonic restraint potential (11) results in the problem of nonlinear optimization in (7), which is solved by the iterative technique. It is important to note that the derivative of the multiplier $(1 - \sqrt{1 - \tau_a^2})$ in Eq. (11) becomes infinite at the limit $\tau_a \to 1$ (although the expression itself approaches unity), which guarantees the existence of the solution of our minimization problem at any nonzero interatomic distance. So the QMPFF method avoids the famous polarization catastrophe.[21,22]

C. Parameters

It is important to note that since the QMPFF method was designed for biomolecular and drug design applications, it is parametrized using only small organic molecules, with the benzene dimer being the largest system in the training set,

TABLE IV. Properties of graphite crystal in *AB* stacking: Exfoliation energy E_{ex}, equilibrium interlayer separation R_0, and *c*-axis elastic constant c_{33}.

	E_{ex} (meV/atom)	R_0 (Å)	c_{33} (GPa)
QMPFF	54.9	3.486	40.6
Experiment	52±5[a]	3.354[b]	40.7[c]

[a]The most recent estimate from Ref. 3. Also the values of 43 (Ref. 1) and 35^{+15}_{-10} (Ref. 2) were reported.
[b]Reference 23.
[c]Estimated value at 0 K from Ref. 25. Room temperature value of 36.5±1.0 was reported in Ref. 26.

and no forms of pure carbon being included. In general, the *ab initio* QM data against which the QMPFF is parametrized are calculated at the second-order Møller-Plesset perturbation theory (MP2) level, but as MP2 is known to be inadequate for π-π interactions, for the benzene dimer we have used values determined by the CCSD(T) method.[18,19] The QMPFF method successfully reproduces both the total QM interaction in the benzene dimer as distance is varied [see Fig. 1(c)] and all the main energy components ES, EX, and DS.[17] The FF also reproduces the QM values for the quadrupole moment and polarizability tensor of benzene and naphthalene. Finally, the model is very applicable to the second virial coefficient of benzene vapor and also to properties of crystals and liquids of PAHs.[17]

All the QMPFF parameters relevant for the systems considered in this research are listed in Tables I and II.

III. RESULTS

A. Graphite crystal

First, the system of two graphene sheets was investigated at *AB* and *AA* registrations. In the *AB* stacking half of the carbons lie directly over an atom in the adjacent layer [*A* type on Fig. 1(d)], while the other half lie over the empty centers of the hexagons of the neighboring plane [*B* type, Fig. 1(d)]. In the less stable *AA* form, all atoms lie over one another, i. e., the whole sheet is translated upward. Table III presents the interaction energy and its components at the optimum interlayer separation. It was found, despite the neutrality of every atom, that the ES contribution is comparable with the others. This is a clear manifestation of the penetration effect, which is demonstrated in more detail in Fig. 1(d). On the other hand, the nonadditivity turns out to be negligible (less than 0.1 meV/atom). As expected, *AB* stacking is more favorable (by 4%) than *AA* and 0.044 Å tighter.

Due to additional interactions with distant layers, the exfoliation energy of bulk graphite is 10% larger compared to interaction of two layers (see Table III). Accordingly, the interlayer separation is 0.033 Å smaller, for the *AB* conformation. The *AA* conformation becomes slightly stiffer: R_0 decreases by only 0.031 Å from two layers to bulk, i.e., 6% less than in *AB* registration.

The energy difference between the *AA* and *AB* registrations influences the behavior of different nanodevices such as bearings or motors. The QMPFF prediction of 2.2 meV/atom is significantly smaller than the DFT result of 15 meV/atom[24] but almost an order of magnitude larger than the value of 0.3 meV/atom predicted by the Lennard-Jones potential.[24] On the other hand, the QMPFF estimate agrees reasonably well with the energy difference between sandwich and PD conformations of benzene dimer found at the CCSD(T) QM level to be 43 meV,[18,19] or 3.6 meV/atom (including hydrogens).

Table IV compares QMPFF predictions for graphite crystal properties with experimental findings. It is seen that the exfoliation energy and elastic constant (inverse compressibility along the axis orthogonal to the basal plane) are in full agreement with experiment. Interlayer separation is reproduced somewhat less accurately, but twofold better than the DFT result of 3.6 Å from Ref. 27, where E_{ex} =48 meV/atom was found. Several alternative DFT calculations have resulted in values of R_0 closer to experiment, but at the expense of severalfold errors in E_{ex} and/or c_{33} (see Ref. 4). The graphite cleavage energy needed to split the crystal in two has also been calculated. The QMPFF method predicts the value of 61.8 meV/atom, i.e., 13% larger than E_{ex}. This relative increase falls in the range between 6% from Ref. 27 and 18% from Ref. 1.

B. Adsorption of PAHs on graphite

Table V presents results of the PAH-graphite system op-

TABLE V. QMPFF predictions for optimal separation R_0 between graphite basal plane and adsorbate, interaction energy *E*, and its components. For two C_{60} orientations, R_0 corresponds to the distance from graphite to the nearest fullerene face denoted in the second column. The last line corresponds to the energy per molecule in C_{60} crystal. All energies are in eV.

Adsorbate	Stacking	R_0 (Å)	*E*	ES	EX	DS
Benzene	*AB*	3.444	−0.46	−0.33	0.55	−0.67
Naphthalene	*AB*	3.454	−0.73	−0.53	0.88	−1.08
Coronene	*AB*	3.471	−1.58	−1.19	1.95	−2.34
Ovalene	*AB*	3.475	−2.07	−1.56	2.55	−3.06
Fullerene C_{60}	*AB* pentagon	3.169	−0.92	−0.52	0.91	−1.31
Fullerene C_{60}	*AB* hexagon	3.188	−0.97	−0.57	0.98	−1.38
Fullerene C_{60}	Crystal		−2.01	−1.23	2.18	−2.96

TABLE VI. Binding energies of various adsorbates to the graphite surface. All energies are in eV.

	Benzene	Naphthalene	Coronene	Ovalene	Fullerene C_{60}
QMPFF	0.46	0.73	1.58	2.07	0.97
Experiment	0.50(8)[a]	0.85(15)[a]	1.4(3)[a]	2.1(3)[a]	0.85(15)[c]
DFT	0.50[b]	0.76[b]			

[a]Reference 3. Uncertainty in last digit(s) is shown in parentheses.
[b]Reference 27.
[c]Reference 28. A clear uncertainty was not reported, so the value for naphthalene is suggested here.

timization. It is seen that the optimal separation is somewhat smaller compared to R_0 in bulk graphite crystal and increases with the size of the PAH. Similarly to the pure graphite case, the ES term is comparable with the others, and once again polarization is negligible. The interaction energy depends almost linearly on the number of carbons or all atoms in a molecule. Comparison of our results with experiment and DFT calculations can be found in Table VI. The deviations from experiment are in the range of experimental uncertainty for all studied cases. It is important to note the equal agreement with experiment irrespective of molecular size, which is another demonstration of QMPFF transferability.

In a strict sense the "experimental" value for graphite exfoliation energy from Ref. 3 should be considered as a theoretical prediction based on a FF (referred to below as the ZFF) fitted to the actual experimental data on PAH-graphite binding energies. The ZFF is pairwise additive, treats atoms as spherically symmetric, and entirely neglects electrostatics. In contrast, the QMPFF is polarizable and accounts for the anisotropic nature of π orbitals and the electrostatic penetration effect. Hence, it is particularly encouraging that such different FFs are both consistent with the PAH experimental data (with the proviso that the ZFF was trained on these data, while the QMPFF is tested on it) and predict almost identical E_{ex} for graphite. Such agreement undoubtedly raises the confidence in both predictions.

C. Fullerene C_{60}

A FF for nanosimulations should describe not only planar structures like graphene, but also caged ones (fullerenes). To demonstrate QMPFF transferability, fullerene C_{60} adsorbed on a graphite surface was considered in two orientations: with either a pentagon or a hexagon face parallel to and closest to the surface. Table V (rows 5 and 6) shows that the former is 5% less stable, though 0.019 Å tighter. There is a significant (by 20%) increase of the relative contribution of the DS energy component for adsorbed fullerene compared to PAHs. This can be rationalized in terms of the increased average interatomic separation: both EX and penetration ES fall off exponentially with distance, while DS decreases more slowly by a power law. The QMPFF prediction for binding energy is in a reasonable agreement with experiment (see Table VI).

To demonstrate the nonadditive nature of the QMPFF, the polarizability of C_{60} was calculated. The deviation from experiment (see Table VII) is well within the range of experimental uncertainty. Our result agrees also with the DFT value of 82 Å^3.[36]

The solid state of fullerene C_{60} was also studied by the QMPFF method. Table VII compares our results with experiment. Both the lattice constant and bulk modulus are in very good agreement with experimental results. The cohesion energy was found to be 8% larger than the experimental value. This discrepancy can be considered as a measure of the difference in properties between carbon in graphite and fullerene. It is enough to reduce the dispersion intensity for C_{60} by only 5% (cf. Table V) to fit experiment. This correction (very small compared to the 32% difference between graphite and fullerene DS parameters from Ref. 37) would simultaneously shift the C_{60} to graphite adsorption energy toward the experimental value (see Table VI).

On the other hand our result of 2.01 eV for E_{coh} is almost identical to the value of 1.99 eV for the FF from Ref. 38, which is known as one of the best empirical potentials for solid C_{60}. This slight discrepancy between theory and experiment can arise, for example, from a rather strong anharmonicity of the C_{60}-C_{60} potential, which makes the $2kT$ correc-

TABLE VII. Properties of solid C_{60}: cohesion energy per molecule E_{coh}, lattice constant a, and bulk modulus B_0. Also the table includes the polarizability α of an isolated C_{60}.

	E_{coh} (eV)	a (Å)	B_0 (GPa)	α (Å^3)
QMPFF	2.01	13.97	18.2	79.0
Experiment	1.86(6)[a]	14.05[b]	18(2)[c]	77(8)[d]

[a]This value is the sublimation enthalpy $\Delta H=1.74(6)$ eV (Ref. 29) measured at $T=707$ K corrected for a conventional $2kT=0.12$ eV contribution for rigid body thermal oscillations (Ref. 30).
[b]Reference 31.
[c]Reference 32, at room temperature. Other reported experimental values are 14(2) (Ref. 33) and 20(5) (Ref. 34).
[d]Reference 35.

tion for thermal motion underestimated at high temperatures.

IV. CONCLUSIONS

In summary, it is demonstrated in this paper that the QMPFF fitted to high-level *ab initio* QM data on the benzene dimer successfully reproduces both bulk graphite experimental properties and PAH binding energies to a graphite surface. Moreover, the model transfers quite well to the fullerene C_{60}.

In all studied systems, the penetration electrostatic effect was found to be important and comparable with the total interaction energy.

Also, the QMPFF prediction of relatively large 55 meV/atom exfoliation energy of graphite provides an independent confirmation of the 52 ± 5 meV/atom value reported in Ref. 3.

Taking into account the very general character of the QMPFF and its potential applicability to all elements and thus to doped carbon structures, it is expected to be of value in computer simulations of hydrogen storage media for fuel cells, nanodevices, and so on.

ACKNOWLEDGMENTS

The author thanks V. I. Tarasov and O. V. Khoruzhii for helpful discussions and C. Queen for careful review of the manuscript. All the formulas from Sec. II have been obtained in close collaboration with V. I. Tarasov.

*Electronic address: alexander.donchev@algodign.com

[1] L. A. Girifalco and R. A. Lad, J. Chem. Phys. **25**, 693 (1956).
[2] L. X. Benedict, N. G. Chopra, M. L. Cohen, A. Zettl, S. G. Louie, and V. H. Crespi, Chem. Phys. Lett. **286**, 490 (1998).
[3] R. Zacharia, H. Ulbricht, and T. Hertel, Phys. Rev. B **69**, 155406 (2004).
[4] M. Hasegawa and K. Nishidate, Phys. Rev. B **70**, 205431 (2004).
[5] J. Zhao, A. Buldum, J. Han, and J. P. Lu, Nanotechnology **13**, 195 (2002).
[6] Y.-H. Kim, Y. Zhao, A. Williamson, M. J. Heben, and S. B. Zhang, Phys. Rev. Lett. **96**, 016102 (2006);.
[7] A. I. Kolesnikov, J.-M. Zanotti, C.-K. Loong, P. Thiyagarajan, A. P. Moravsky, R. O. Loutfy, and C. J. Burnham, Phys. Rev. Lett. **93**, 035503 (2004).
[8] D. Lu, Y. Li, U. Ravaioli, and K. Schulten, Phys. Rev. Lett. **95**, 246801 (2005).
[9] Q. Wang and J. K. Johnson, J. Chem. Phys. **110**, 577 (1999).
[10] M. Hirscher, M. Becher, M. Haluska, A. Quintel, V. Skakalova, Y.-M. Choi, U. Dettlaff-Weglikowska, S. Roth, I. Stepanek, P. Bernier, A. Leonhardt, and J. Fink, J. Alloys Compd. **330–332**, 654 (2002).
[11] S. Patchkovskii, J. S. Tse, S. N. Yurchenko, L. Zhechkov, Th. Heine, and G. Seifert, Proc. Natl. Acad. Sci. U.S.A. **102**, 10439 (2005).
[12] J. T. Sprague and N. L. Allinger, J. Comput. Chem. **1**, 257 (1980).
[13] N. L. Allinger and J.-H. Lii, J. Comput. Chem. **8**, 1146 (1987).
[14] T. A. Halgren, J. Comput. Chem. **17**, 490 (1996).
[15] A. G. Donchev, V. D. Ozrin, M. V. Subbotin, O. V. Tarasov, and V. I. Tarasov, Proc. Natl. Acad. Sci. U.S.A. **102**, 7829 (2005).
[16] A. G. Donchev, N. G. Galkin, A. A. Illarionov, O. V. Khoruzhii, M. A. Olevanov, V. D. Ozrin, M. V. Subbotin, and V. I. Tarasov Proc. Natl. Acad. Sci. U.S.A. **103**, 8613 (2006).
[17] A. G. Donchev, N. G. Galkin, L. Preyaslavets, and V. I. Tarasov (to be published).
[18] S. Tsuzuki, K. Honda, M. Mikami, and K. Tanabe, J. Am. Chem. Soc. **124**, 104 (2002).
[19] M. O. Sinnokrot, E. F. Valeev, and C. D. Sherrill, J. Am. Chem. Soc. **124**, 10887 (2002).
[20] K. T. Tang and J. P. Toennies, J. Chem. Phys. **80**, 3726 (1984).
[21] B. T. Thole, Chem. Phys. **59**, 341 (1981).
[22] P. Th. van Duijnen and M. Swart, J. Phys. Chem. A **102**, 2399 (1998).
[23] N. N. Greenwood and A. Earnshaw, *Chemistry of the Elements* (Pergamon, New York, 1984).
[24] A. N. Kolmogorov and V. H. Crespi, Phys. Rev. B **71**, 235415 (2005).
[25] W. B. Gauster and I. J. Fritz, J. Appl. Phys. **45**, 3309 (1974).
[26] O. L. Blakslee, D. G. Proctor, E. J. Seldin, G. B. Spence, and T. Weng, J. Appl. Phys. **41**, 3373 (1970).
[27] S. D. Chakarova-Käck, E. Schröder, B. I. Lundqvist, and D. C. Langreth, Phys. Rev. Lett. **96**, 146107 (2006).
[28] H. Ulbricht, G. Moos, and T. Hertel, Phys. Rev. Lett. **90**, 095501 (2003).
[29] C. Pan, M. P. Sampson, Y. Chai, R. H. Hauge, and J. L. Margrave, J. Phys. Chem. **95**, 2944 (1991).
[30] W. T. M. Mooij, B. P. van Eijck, and J. Kroon, J. Phys. Chem. A **103**, 9883 (1999).
[31] R. Sachidanandam and A. B. Harris, Phys. Rev. Lett. **67**, 1467 (1991).
[32] S. J. Duclos, K. Brister, R. C. Haddon, A. R. Kortan, and F. A. Thiel, Nature (London) **351**, 380 (1991).
[33] J. E. Fischer, P. A. Heiney, A. R. McGhie, W. J. Romanow, and A. M. Denenstein, Science **252**, 1288 (1991).
[34] S. Hoen, N. G. Chopra, X.-D. Xiang, R. Mostovoy, J. Hou, W. A. Vareka, and A. Zettl, Phys. Rev. B **46**, 12737 (1992).
[35] R. Antoine, P. Dugourd, D. Rayane, E. Benichou, M. Broyer, F. Chandezon, and C. Guet, J. Chem. Phys. **110**, 9771 (1999).
[36] G. K. Gueorguiev, J. M. Pacheco, and D. Tománek, Phys. Rev. Lett. **92**, 215501 (2004), and references therein.
[37] L. A Girifalco, M. Hodak, and R. S. Lee, Phys. Rev. B **62**, 13104 (2000).
[38] X.-P. Li, J. P. Lu, and R. M. Martin, Phys. Rev. B **46**, 4301 (1992).
[39] E_{ex} is almost identical to the cohesion energy needed to separate all layers of the graphite crystal to infinity. A slight difference between the two quantities can arise from electron polarization, which is zero by symmetry for bulk atoms but shows up for surface ones. An alternative source of the difference is a small increase of interlayer separation near the surface. In the present research both the effects were found to be energetically negligible, though the latter indeed takes place and the surface layer moves away by 0.018 Å. So we will not distinguish exfoliation and cohesion graphite energy.